Catalysis Today 145 (2009) 127–137

Contents lists available at ScienceDirect

Catalysis Today

journal homepage: www.elsevier.com/locate/cattod

Composite catalytic materials for steam reforming of methane and oxygenates: Combinatorial synthesis, characterization and performance

Vladislav Sadykov [a,*], Natalia Mezentseva [a], Galina Alikina [a], Rimma Bunina [a], Vladimir Rogov [a], Tamara Krieger [a], Sergey Belochapkine [b], Julian Ross [c]

[a] Boreskov Institute of Catalysis, 5 Pr. Lavrentieva, 630090 Novosibirsk, Russia
[b] Materials & Surface Science Institute, University of Limerick, Limerick, Ireland
[c] Centre of Environmental Research, University of Limerick, Limerick, Ireland

ARTICLE INFO

Article history:
Available online 13 June 2008

Keywords:
Composites
Ni–YSZ
Doped ceria–zirconia oxides
Ru
Steam reforming
CH_4
Ethanol
Acetone

ABSTRACT

Using robotic workstation, a number of composite materials based on NiO/yttria-doped zirconia (YSZ) cermet promoted with doped ceria–zirconia fluorite-like mixed oxides and Ru were synthesized. The materials were characterized by XRD, BET, TEM, H_2 TPR, and their catalytic performance was estimated in the reactions of methane, ethanol and acetone steam reforming at short (10–36 ms) contact times. The amount of deposited carbonaceous species was estimated by temperature-programmed oxidation. Complex fluorite-like oxides as promoters minimize coking even in stoichiometric fuel/steam feeds. Promotion by small (<1 wt.%) amount of Ru further decreases coking and facilitates activation of such molecules as CH_4 and acetone, thus ensuring a high level of performance in the intermediate temperature (500–600 °C) range. Factors controlling performance of these composites in steam reforming reactions such as lattice oxygen mobility in complex oxide promoters controlled by their chemical composition, strong interaction between components in composites, state and reactivity of supported Ru were assessed.

1. Introduction

In the last years biomass has been recognized as one of the major world renewable energy sources. Bio-oil derived from the fast pyrolysis of biomass or bio-ethanol can be converted via steam reforming into hydrogen or syngas, which can be further used in fuel cells for power generation or directed to synthesis of liquid fuels (gasoline and diesel) and valuable chemicals [1,2]. For solid oxide fuel cells, an attractive option is direct internal reforming of biofuels on catalytically active anodes [3]. Hence, efficient, inexpensive and robust catalysts for the steam reforming of biofuel are required. To improve the overall efficiency of biofuels transformation into synfuels or energy, the steam excess in these endothermic processes should be kept to a minimum. However, the most demanding problem of their design is heavy coking of catalysts even in the feeds with excess of steam caused by a high reactivity of biofuel components (carboxylic acids, aldehydes, ketones, alcohols and phenols), thus excluding application of traditional Ni-based steam reforming catalysts [4], Ni–yttria-doped zirconia (YSZ) anode cermets [3] or precious metals (Pt, Pd and Ru) supported on traditional carriers with developed surface area (alumina and zirconia [5,6]). A promising approach to design of steam reforming catalysts resistant to coking consists in synthesis of nanocomposites comprised of components able to efficiently activate C–H and C–C bonds in the fuel molecules (Ni, precious metals) and oxide components providing activation of water molecules and transfer of hydroxyls and/or hydroxocarbonate/oxygen species to the metal particles where they interact with activated C–H–O species producing syngas [4,7–9]. Basic oxides such as lanthana [4,10], ceria [11], yttria [12], zirconia [13], ceria–zirconia [14–16], etc. were shown to be quite efficient in this respect. Recently, modification of traditional Ni/YSZ anode cermets with ceria–zirconia fluorite-like solid solutions doped by Pr, La or Gd was shown to suppress their coking in stoichiometric methane–steam feeds, while supporting small (~1 wt.%) amounts of precious metals (Pt, Ru and Pd) allowed to provide a high performance in the intermediate temperature range (500–600 °C) at short (milliseconds) contact times [17–19]. Such inexpensive composites could be also attractive as active components of catalysts for steam reforming of biofuels, though this has not been properly verified up to date. To ensure a high performance of these composites in steam reforming of a given type of biofuel component, their composition

* Corresponding author. Tel.: +7 38333 08763; fax: +7 38333 08056.
E-mail address: sadykov@catalysis.ru (V. Sadykov).

0920-5861/$ – see front matter © 2008 Elsevier B.V. All rights reserved.
doi:10.1016/j.cattod.2008.04.034

and preparation procedures are to be properly optimized, first of all, as related to the type and content of doping cations in fluorite-like ceria–zirconia solid solutions controlling mobility and reactivity of the surface and bulk oxygen species [20,21]. In this respect, application of the combinatorial synthesis procedures using robotic workstations [22] which provide unique possibilities of fast preparation of a large number of samples required for such optimization seems to be very promising.

Hence, this paper presents results of research aimed at design of active components of catalysts for steam reforming of biofuel components (ethanol and acetone) comprised of YSZ + NiO + complex fluorite-like doped ceria–zirconia oxides + Ru. Selection of acetone along with ethanol stems from the fact that acetone is formed as an intermediate product during steam reforming of ethanol [5] or acetic acid [23]—typical components of bio-oil. Namely subsequent steps of acetone transformation on oxide supports are considered as being responsible for the catalysts coking [23]. Similarly, cracking of ethanol in the course of steam reforming is known to produce methane [5], which, as the most stable alkane, could limit the total degree of ethanol conversion into hydrogen/syngas. This consideration determined selection of methane as the third compound to be tested in steam reforming reaction over prepared series of composite catalysts. Since all these compounds strongly differ by their chemical stability, nature of functional groups and reactivity, comparison of results obtained for the same series of catalysts in transformation of different molecules could provide valuable information about the structural sensitivity of respective reactions related to the nature of their rate-limiting stages.

Based upon results of our previous research for doped ceria–zirconia (1:1) solid solutions [16–21], Pr was chosen here as a dopant providing the highest surface/bulk lattice oxygen mobility due to formation of Pr^{3+}/Pr^{4+} redox pairs. However, at a high (30 at.%) Pr content a strong Pr segregation in the surface layer was observed, which might result in too strong interaction with supported precious metals leading to stabilization of their oxidic forms less reactive in activation of fuel components [17,18]. To check this hypothesis, in this work, Pr was incorporated into ceria–zirconia solid solution along with bigger (La^{3+}) or smaller (Sm^{3+}) cations which were also found to be quite efficient dopants increasing lattice oxygen mobility [19]. This allows to control also the acid–base properties of these complex oxide promoters determining mobility and reactivity of surface hydroxyls and hydroxocarbonates and check their effect on catalytic properties. Moreover, in this work, Ce/Zr ratio was also tuned to elucidate the effect of the overall content of reducible cations in doped ceria–zirconia complex oxides on their efficiency as promoters.

Selection of Ru as a co-promoter along with the fluorite-like oxides was primarily determined by its lowest price among precious metals which is a very important factor for any possible practical application. At least, in partial oxidation of ethanol on Pd- or Ru-supported yttria, Ru was found to be much more efficient than Pd [12].

To elucidate the effect of the lattice oxygen mobility on performance of composites in steam reforming reactions, H_2 TPR was applied for its characterization, while the temperature-programmed oxidation (TPO) of samples discharged after reaction was used to characterize the amount and reactivity of deposited carbonaceous species.

From the practical point of view, the most efficient and robust catalytic compositions could also be used for design of catalytically active anodes of solid oxide fuel cells operating in regimes of direct internal reforming of methane and/or biofuels.

2. Experimental

2.1. Catalysts preparation

The composite anode materials based on 60% NiO–40% YSZ composite promoted with 10 wt.% fluorite-like oxides and Ru (~1 wt.%) were synthesized using robotic workstation based on the Hamilton Microlab Duo system [22] via multistage incipient wetness impregnation followed by drying overnight in air at 90 °C and then calcination at 800 °C and regrinding after each stage. At the first stage, NiO was added to powdered $Y_{0.08}Zr_{0.92}O_{2-y}$ (8YSZ, Russian source) using nitrate solution, then this basic composite was promoted by fluorite-like oxides ($Pr_xCe_yZr_zO_2$, $La_qPr_xCe_yZr_zO_2$, $Sm_qPr_xCe_yZr_zO_2$, where $y = 0.35, 0.5$; $z = 0.35, 0.25, 0.2$; $x = 0.15$–0.3; $q = 0.15$) using respective mixed nitrates solutions. At last, Ru (0.9 wt.% or 1.3 wt.%) was supported on complex oxides promoted composites by impregnation with $RuCl_3$ solution followed by calcination at 800 °C.

2.2. Catalysts characterization

The specific surface area (BET area) was determined by the express BET method using Ar thermodesorption data obtained on a SORBI-M instrument.

The TEM micrographs were obtained with a JEM-2010 instrument (lattice resolution 1.4 Å) and acceleration voltage 200 kV. Local elemental analysis was performed with EDX method (a Phoenix Spectrometer).

The XRD patterns were recorded using an URD-6M diffractometer with Cu Kα radiation in the range of 2θ angles 10–90°.

H_2 TPR experiments were carried out for samples pretreated in O_2 at 500 °C using feed containing 10 vol.% H_2 in Ar at flow rate 40 ml min^{-1} and temperature ramp 10 °C min^{-1} from ~25 °C to 900 °C. During the experiment H_2O was frozen out at −80 °C. The hydrogen concentration was determined using a thermal conductivity detector.

For TPO experiments, samples after achieving a steady-state performance in the steam reforming of acetone or ethanol at the highest temperature of experiments (700 °C), were cooled in the same feed to 500 °C within ~3 h, then cooled to room temperature in a closed reactor, discharged from the reactor and transferred into another one under contact with air. Before TPO run, samples were heated in the stream of He up to 100 °C, kept at this temperature for 0.5 h, then He was changed to 0.5% O_2 in He feed, and temperature was increased up to 880 °C with a ramp of 5 °C/min, products evolution being monitored by PEM-2M gas analyzer as described elsewhere [17].

2.3. Catalyst testing

Catalytic activity in the steam reforming of methane (CH_4 SR) at short contact times (10 ms) was studied using 8% CH_4 + 8–24% H_2O in N_2 feeds for samples (0.5–1 mm fraction) pretreated in O_2 at temperatures up to 850 °C in a flow installation by using a flow quartz reactor and earlier described procedures [16–18].

Catalytic activity in the reactions of ethanol steam reforming (ESR) (standard feed 0.5% C_2H_5OH + 2.5% H_2O in He) at short contact times (36 ms) was estimated in a flow installation by using a flow quartz reactor (internal diameter 2.5 mm) packed with a catalyst (0.25–0.5 mm fraction) diluted with a quartz sand. In these tests catalysts were heated to the temperature of experiment in the flow of 1% O_2 in He, and then the reaction mixture was fed till the stationary concentrations of the products were attained.

Catalytic activity of samples (0.25–0.5 mm fraction) in the acetone steam reforming (ASR) at short contact times (20 ms) was

studied using 0.8% C_3H_6O + 3.5% H_2O in He feed in the temperature range of 500–700 °C. To accelerate attainment of steady-state activity in this reaction at moderate (500–600 °C) temperatures in rather diluted feed containing acetone (less reactive than ethanol), catalysts were subjected to a mild reducing pretreatment (1 h at 500 °C in the stream of 2% H_2 in He) to convert NiO into Ni.

The products (H_2, CO and CO_2) and CH_4 concentrations in converted feeds were continuously monitored by using on-line IR absorbance gas analyzer PEM-2M, TCD and an electrochemical H_2 sensor with the data acquisition and processing through a PC.

In all experiments, a cooled trap kept either at ~−40 °C (for oxygenates steam reforming in diluted feeds) or at 10 °C (for methane steam reforming) was placed at the reactor exit to condense excess water and/or non-reacted oxygenates as well as intermediate products of their transformation (aldehydes, etc.), thus preventing condensation of liquids within analyzers and damage of sensors. Hence, the results obtained in this work with a fixed composition of model diluted reaction feeds are to be considered as mainly aimed at scanning catalytic properties of a library of samples within routine of the combinatorial approach, while more detailed studies of the most promising samples using feeds with realistic compositions will be mainly presented elsewhere.

Catalytic experiments in ethanol steam reforming in a realistic feed (EtOH:H_2O:N_2 = 1:4:5) presented for comparison in this work for one selected sample with the aim to demonstrate typical products distribution for composite catalysts were carried out in U-shaped tubular quartz flow reactor (4.5 mm i.d.) at atmospheric pressure. Usually 0.18 g of pelletized catalyst (fraction 0.5–0.25 mm) diluted in a 1:10 weight ratio with quartz sand was taken. Reaction was performed at 600–800 °C and the total flow rate 9 l/h (contact time ca. 70 ms). Before testing, the catalyst was pretreated for 1 h at 400 °C in the flow of 10% O_2 in N_2. Three on-line gas chromatographs (GC) "LHM-8" equipped with thermal conductivity detectors and a flame ionization detector respectively were used for the analysis of reactants and products. Hydrocarbons (CH_4, C_2H_6, C_2H_4, etc.) and oxygenates (EtOH, CH_3OH, acetone, diethyl ether, acetaldehyde, etc.) were analyzed using a Porapak T column; N_2, O_2, CH_4 and CO were analyzed with a molecular sieve column, and H_2, N_2, CO, CO_2, CH_4 with an active carbon "SYT" column. Ar and He were used as carrier gases.

3. Results and discussion

3.1. Catalysts characterization

3.1.1. Structural characteristics and microstructure of composites

The BET surface area of composite materials was ~9 (±1) m^2/g.

Fig. 1 presents XRD patterns of NiO + YSZ composite, fluorite-like $Pr_{0.15}La_{0.15}Ce_{0.35}Zr_{0.35}O_2$ oxide and NiO + YSZ composite promoted by this oxide. For $Pr_{0.15}La_{0.15}Ce_{0.35}Zr_{0.35}O_2$ oxide prepared via Pechini route [19–21] and calcined at 800 °C, broad diffraction peaks correspond to a cubic fluorite-like phase [JCPDS 89-7130] with small particle sizes. In promoted composite, along with strong reflections corresponding to doped zirconia and NiO phases [17], weak broad reflections of added fluorite-like phase were observed as well. However, in these composites, both before and after supporting doped ceria–zirconia oxide, along with reflections corresponding to cubic/tetragonal YSZ phase [JCPDS 70-4431] (highly dispersed c- or t-ZrO_2 phases are not discerned easily by routine XRD analysis [24]), reflections corresponding to monoclinic zirconia phase [JCPDS 78-1807] were observed as well. As judged by the ratio of reflections intensity, promotion of NiO + YSZ composite by doped ceria–zirconia oxide increases further the content of monoclinic zirconia. This implies that preparation procedure used in our robotic synthesis route, namely, successive impregnation of YSZ powders

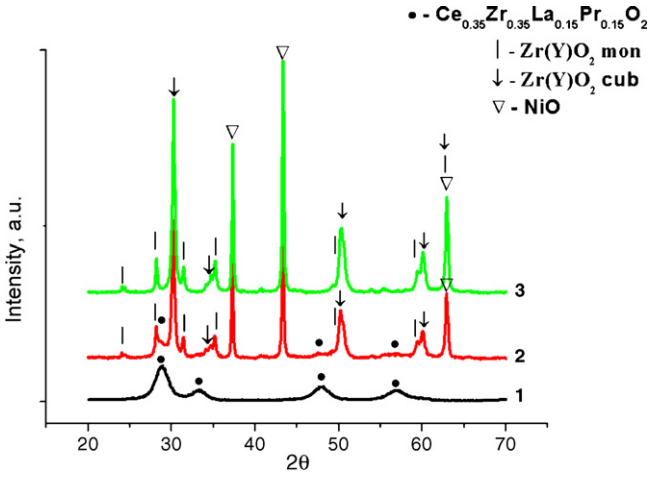

Fig. 1. XRD patterns of $Ce_{0.35}Zr_{0.35}La_{0.15}Pr_{0.15}O_2$ (1), 10% $Ce_{0.35}Zr_{0.35}La_{0.15}Pr_{0.15}O_2$/NiO + YSZ (2) and NiO + YSZ (3).

with the excess of acidic nitrate solutions followed by evaporation to dryness and calcination [22], favors leaching of Y from doped zirconia. This results in destabilization and disordering of the cubic zirconia structure, while at least the surface layers of perovskite-like yttrium nickelates can be formed. Earlier [17], such variation of the structural features of doped zirconia was not observed for NiO + YSZ (ScCeSZ) composites promoted by complex oxides via impregnation with solutions of polymeric polyester precursor (Pechini route).

Fig. 2 demonstrates typical morphology, microstructural features and local composition of composites prepared in this work. Samples are comprised of big (~1 μm) porous aggregates formed by stacking of particles with typical sizes in the range of 10–100 nm strongly differing by contract (Fig. 2a). EDX analysis revealed presence of zirconia particles containing some amounts of elements corresponding to supported doped ceria–zirconia oxide (Fig. 2b) but without any traces of nickel. These zirconia particles are comprised of well-crystallized coherently stacked domains with distances 3.02 Å corresponding to the (1 1 1) planes of cubic zirconia [JCPDS 70-4431] separated by nanopores with walls oriented along the lattice planes. In other regions (Fig. 2c) juxtaposed NiO and fluorite-like oxide particles containing elements corresponding to cations of doped ceria–zirconia oxide are revealed. A distance of 3.4 Å observed in some particles corresponds to the (1 1 1) planes in doped ceria–zirconia oxide with a bigger lattice parameter than in YSZ [19].

A high-resolution image of these regions (Fig. 2d) shows nearly coherently intergrown particles of fluorite-like oxide (mainly, doped zirconia phase in this case) and NiO. EDX analysis revealed considerable incorporation of components corresponding to doped ceria–zirconia phase into zirconia, which is also reflected in the increase of (1 1 1) spacing to 3.08 Å. Simultaneously, presence of some Ni in EDX spectrum suggests that at least the surface layer of fluorite-like phase contains this element, perhaps, as perovskite-like clusters (vide supra), though incorporation of some amount of Ni cations into the lattice of fluorite-like oxides [25,26] and/or into nanopores of YSZ (vide supra) is possible as well. Traces of Zr and Y were also revealed in the regions of NiO particles.

Separate particles of supported Ru were not observed in all samples, which is explained by its low content as well as pronounced interaction with other components of composite (vide infra). Some traces of Ru were revealed by EDX practically in all regions (Fig. 2).

Hence, structural studies revealed pronounced interaction between phases present in composites with detectable variation of the chemical composition of fluorite-like oxide particles.

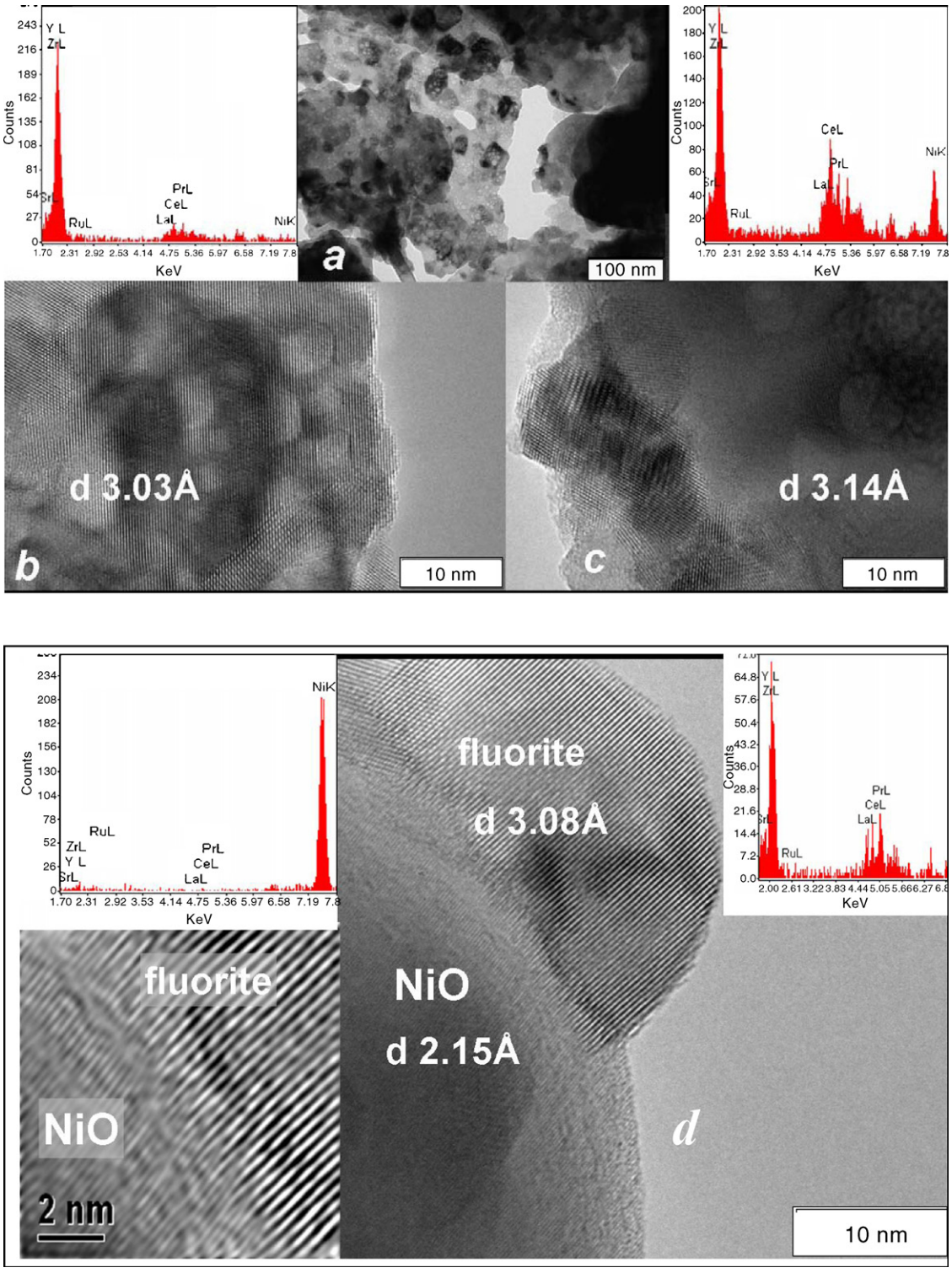

Fig. 2. Typical morphology, microstructure and local composition (by EDX) of NiO + YSZ composite promoted by $Pr_{0.15}La_{0.15}Ce_{0.35}Zr_{0.35}O_2$ oxide and Ru. (a) Macro/mesoporous aggregates of particles; (b) disordered nanodomain ZrO_2 particle containing internal nanopores and respective EDX spectrum; (c) disordered nanodomain particles of fluorite-like oxide promoter on the surface of NiO particle and respective EDX spectrum; (d) contact area between NiO and YSZ particle modified by the elements of complex oxide promoter.

3.1.2. Temperature-programmed reduction

Typical H_2 TPR spectra are shown in Figs. 3–6. For all composites, NiO reduction was completed up to 600–650 °C. For unpromoted NiO + YSZ composite, reduction starts at ~330 °C (Fig. 3), while for pure NiO [10,27] or its mechanical mixture with YSZ [17] it begins already at ~280 °C. Moreover, for both pure NiO and NiO + YSZ mixture, only one reduction peak is observed with T_{max} ~ 350 °C [10,17,27], which is rather close by position to the first reduction peak observed in unpromoted composite (Fig. 3). Hence, this peak can be assigned to reduction of NiO particles non-modified by interaction with YSZ. Reduction peak with a maximum at ~400 °C in the spectrum of unpromoted composite (Fig. 3) is

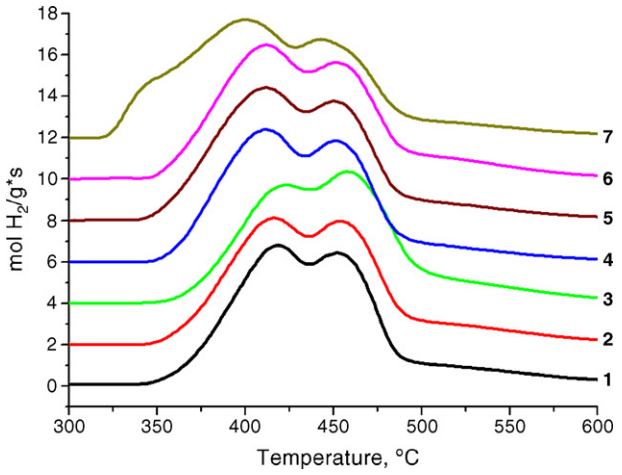

Fig. 3. H_2 TPR spectra of NiO + YSZ-based composites promoted by $Pr_{0.3}Ce_{0.35}Zr_{0.35}O_2$ (1), $Pr_{0.25}Ce_{0.5}Zr_{0.25}O_2$ (2), $Pr_{0.15}La_{0.15}Ce_{0.35}Zr_{0.35}O_2$ (3), $Pr_{0.15}La_{0.15}Ce_{0.5}Zr_{0.2}O_2$ (4), $Pr_{0.15}Sm_{0.15}Ce_{0.35}Zr_{0.35}O_2$ (5), $Pr_{0.15}Sm_{0.15}Ce_{0.5}Zr_{0.2}O_2$ (6) or unpromoted NiO + YSZ (7).

similar by position to peaks earlier observed for NiO supported on CeO_2 [25] and for NiO + YSZ mechanical mixture promoted by $Ce_{0.5}Zr_{0.5}O_2$ oxide [17]. Appearance of this peak was explained by stabilization of Ni^{2+} cations on the surface of NiO particles by decoration with Ce^{4+} cations or CeO_x fragments. TPR peaks with T_{max} situated even at higher (450–600 °C) temperatures were observed in the case of NiO supported on zirconia [27–29], ceria–zirconia [27] or alumina [27]. Moreover, in the case of NiO + $Sc_{0.1}Ce_{0.01}Zr_{0.89}O_{2-y}$ composite sintered into dense pellets and then ball milled into powders, two overlapping peaks with $T_{max} \sim 450$ °C and 500 °C were observed [18]. This suggests that decoration of the surface of NiO particles by irreducible cations (Zr^{4+}, Sc^{3+} and Y^{3+}) and/or strong interaction between particles of NiO and zirconia further hampers NiO reduction. The high-temperature (up to 700 °C) tail of hydrogen consumption observed for undoped composite (Fig. 3, curve 7), by analogy with published data [25–29], can be assigned to reduction of Ni cations incorporated into the bulk of doped zirconia particles, perhaps, primarily being located within nanopores detected by TEM (vide supra). Hence, TPR data revealed pronounced variation of the reactivity of NiO particles/species in unpromoted NiO + YSZ composite, which could reflect different degree of chemical interaction between components.

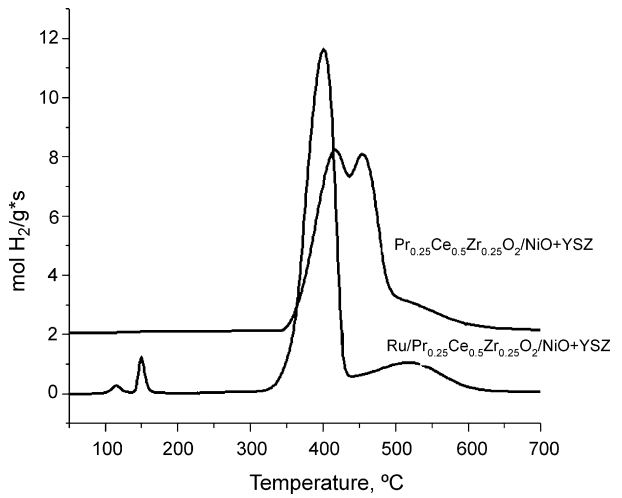

Fig. 4. Effect of Ru-supporting on H_2 TPR spectra of $Pr_{0.25}Ce_{0.5}Zr_{0.25}O_2$/NiO + YSZ composite.

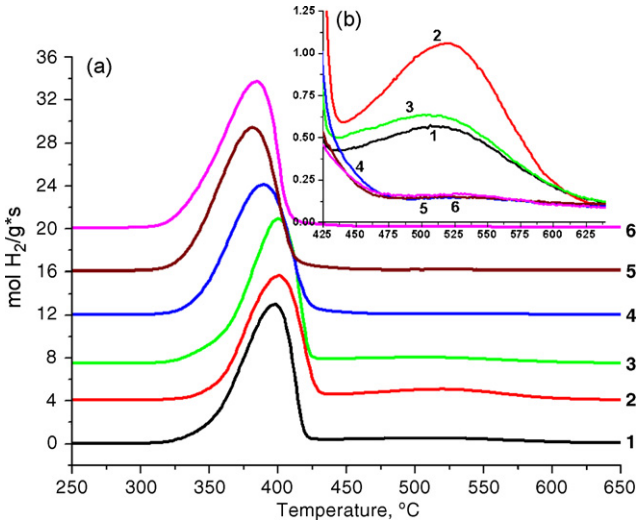

Fig. 5. H_2 TPR spectra of composites co-promoted with 0.9 wt.% Ru and $Pr_{0.3}Ce_{0.35}Zr_{0.35}O_2$ (1), $Pr_{0.25}Ce_{0.5}Zr_{0.25}O_2$ (2), $Pr_{0.15}La_{0.15}Ce_{0.35}Zr_{0.35}O_2$ (3), $Pr_{0.15}La_{0.15}Ce_{0.5}Zr_{0.2}O_2$ (4), $Pr_{0.15}Sm_{0.15}Ce_{0.35}Zr_{0.35}O_2$ (5) and $Pr_{0.15}Sm_{0.15}Ce_{0.5}Zr_{0.2}O_2$ (6).

Supporting complex oxides practically eliminates the first TPR peak situated at ~350 °C (Fig. 3), slightly shifts the second peak to higher temperatures and increases the relative share of the high-temperature peak at ~470 °C. A high-temperature reduction tail extending up to 700 °C remains to be observed for all samples. This implies that the second impregnation provides modification of the surface of all NiO particles present in composite by Zr and rare-earth cations. More detailed analysis of reduction patterns agrees with this suggestion. Thus, the biggest share of the second high-temperatures peak is found for composite promoted by $Pr_{0.15}La_{0.15}Ce_{0.35}Zr_{0.35}O_2$ complex oxide containing La. Indeed, this could favor appearance of perovskite-like lanthanum nickelate fragments on the surface of NiO particles. According to known data [10,30], supported La–Ni–O oxides are intensively reduced only at temperatures exceeding 600 °C. Similarly, incorporation of Ni cations into the bulk of doped ceria–zirconia particles [25,26]

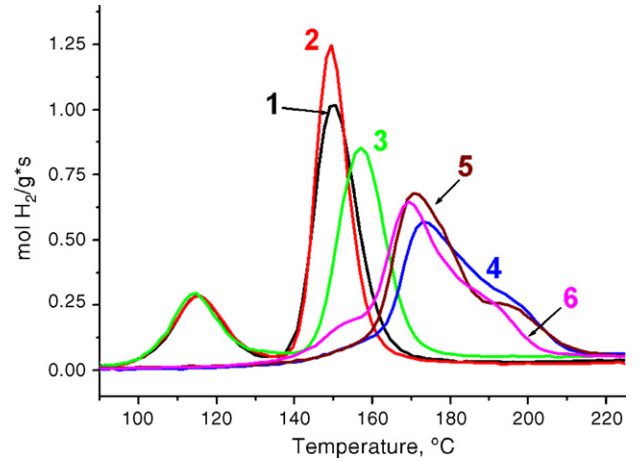

Fig. 6. H_2 TPR spectra of composites co-promoted with Ru (0.9 wt.%) and fluorite-like oxides (1, $Pr_{0.3}Ce_{0.35}Zr_{0.35}O_2$; 2, $Pr_{0.25}Ce_{0.5}Zr_{0.25}O_2$; 3, $Pr_{0.15}La_{0.15}Ce_{0.35}Zr_{0.35}O_2$; 4, $Pr_{0.15}La_{0.15}Ce_{0.5}Zr_{0.2}O_2$; 5, $Pr_{0.15}Sm_{0.15}Ce_{0.35}Zr_{0.35}O_2$; 6, $Pr_{0.15}Sm_{0.15}Ce_{0.5}Zr_{0.2}O_2$) corresponding to reduction of different oxidic forms of Ru in the low-temperature range.

could be another reason for appearance of NiO_x species reduced only at high temperatures.

On the other hand, increasing content of red-ox cations (Ce and Pr) in supported fluorite-like oxides and replacing La by Sm somewhat facilitates reduction as revealed by shift of the first peak to lower temperatures and increasing its share (Fig. 3). Since reduction of NiO into Ni is well known to be a topochemical process occurring through generation of Ni° phase nuclei at some specific highly reactive sites (usually, located at outlets of extended defects such as dislocations, etc.) with their subsequent growth, in fact, oxide additives should not cover all the surface of NiO particles by a dense layer to cause noticeable effect on their reduction characteristics. It is sufficient to decorate a small number of surface defect sites in vicinity of the dislocation outlet or domain/grain boundaries to hamper or accelerate removal of oxygen from these sites, and, hence, dynamics of Ni° nucleation, thus shifting TPR peak position upward or downward, respectively. Indeed, promotion of NiO reduction by Ce cations was detected by Srinivas et al. [26].

Promotion of composites by Ru clearly accelerates their reduction by hydrogen (Figs. 4 and 5) characterized by the main peak situated at 370–400 °C and increases the total degree of samples reduction achieved during TPR run up to 900 °C (Table 1). In general, promoting effect of supported Pt group metals on the oxides reduction by hydrogen is a well-documented phenomenon explained by the efficient activation of H_2 molecules on the metal particles and spill-over of atomic hydrogen onto the oxide surface, thus easily removing reactive oxygen forms [31]. Downward shift of H_2 TPR peak is observed for any mechanism of the solid oxide reduction, either topochemical (such as NiO reduction) or diffusion-controlled (reduction of ceria–zirconia solid oxide solution) [31]. Facilitation of the lattice oxygen mobility due to incorporation of precious metals into domain boundaries and subsurface layers is demonstrated as well [32].

In addition, for Ru-promoted samples, in the low-temperature (100–230 °C) range, new peaks appear (Fig. 5) apparently corresponding to reduction of different Ru oxidic species [13,33,34]. For Ru supported on ceria or zirconia, peaks assigned to reduction of RuO_2 species with different dispersion are situated at 80–100 °C [13,34]. Hence, TPR peaks at 115–150 °C observed for some samples (Fig. 6, curves 1–3) suggest rather weak interaction of RuO_x species with other phases present in composites. When Ru cations are incorporated into the surface vacancies of La–Sr–chromate with the perovskite structure, these peaks are shifted to higher (180–200 °C) temperatures [33]. Hence, peaks observed at ~170 °C for composite samples promoted by complex fluorites containing Sm cations and a larger fraction of reducible cations (Ce and Pr), can be assigned to reduction of RuO_x species strongly interacting with these oxidic promoters, perhaps, modified also by dissolved Ni cations (Fig. 6, curves 4–6). This interaction apparently facilitates reduction of NiO present in promoted composites, since for the latter samples T_{max} of the main reduction peak is shifted downward (Fig. 5a), and the total amount of consumed hydrogen increases (Table 1) despite disappearance of the low-intense broad reduction peak at ~500 °C (Fig. 5b) assigned to reduction of Ni and/or Ce^{4+}/Pr^{4+} cations in the bulk of fluorite-like oxide particles. This implies that both Ru and promoting fluorite-like oxides are rather uniformly distributed within composite decorating NiO particles and, perhaps, even incorporating into domain boundaries/interfaces of oxide particles.

Table 1
Effect of chemical composition of composite materials on hydrogen consumption (mmol H_2/g_{Cat}) in different temperature ranges

Catalyst	Without Ru	+0.9 wt.% Ru	
Temperature range (°C)	40–900	40–230	230–900
NiO + YSZ	6.37	–	–
$Pr_{0.3}Ce_{0.35}Zr_{0.35}O_2$/NiO + YSZ	6.33	0.19	6.18
$Pr_{0.25}Ce_{0.5}Zr_{0.25}O_2$/NiO + YSZ	6.21	0.19	6.24
$Pr_{0.15}La_{0.15}Ce_{0.35}Zr_{0.35}O_2$/NiO + YSZ	6.20	0.19	6.35
$Pr_{0.15}La_{0.15}Ce_{0.5}Zr_{0.2}O_2$/NiO + YSZ	6.00	0.17	6.13
$Pr_{0.15}Sm_{0.15}Ce_{0.35}Zr_{0.35}O_2$/NiO + YSZ	6.20	0.19	6.45
$Pr_{0.15}Sm_{0.15}Ce_{0.5}Zr_{0.2}O_2$/NiO + YSZ	6.25	0.18	6.43

3.2. Catalytic performance

3.2.1. Methane steam reforming

In the reaction of methane steam reforming in the stoichiometric feed, in studied temperature range, performance of Ni–YSZ composites promoted by fluorite-like oxides (both with and without Ru) was in general stable at least for several hours at each temperature. This stability is achieved despite accumulation of some amount of coke on the surface, which is the most efficiently hampered by combination of complex oxide and precious metal promoters [17]. To illustrate the scale of specific catalytic activity of composites in this reaction, the efficient first-order reaction rate constants estimated for the plug-flow reactor following earlier suggested routine [17] are given in Figs. 7 and 8. The values of efficient rate constants varying in the range of 10–30 s^{-1} at 600 °C demonstrate a high specific activity of these composites in the middle-temperature range required for their application as catalytically active anodes of solid oxide fuel cells operating in regimes of direct internal reforming of methane [17].

Performance of composites without Ru strongly depends on composition of the oxide additives (Fig. 7). The most important feature is a rather high middle-temperature activity of some composites in stoichiometric feed even without addition of precious metals, which was not observed earlier for Ni–YSZ based composites [17,18]. This seems to be provided by a strong interaction of promoting fluorite-like oxides with NiO particles due to specificity of the preparation route (vide supra) as well as by their specific chemical composition, namely, a high fraction of reducible Ce and Pr cations along with basic La and Sm cations affecting the oxygen mobility in composites. This implies that a good performance in methane steam reforming in the middle-temperature range in stoichiometric feed can be provided by Ni as

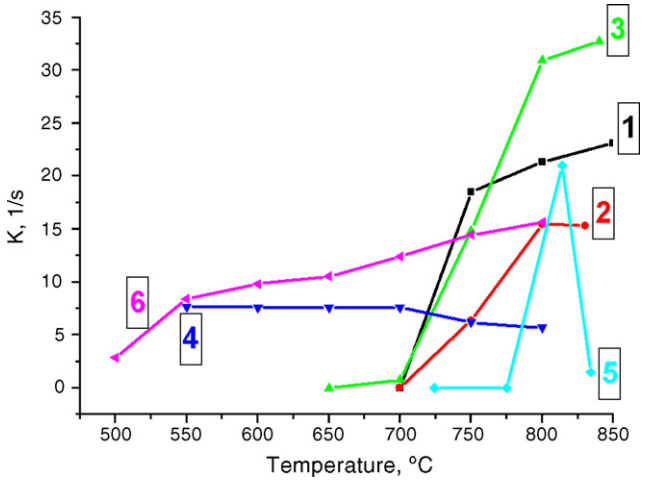

Fig. 7. Efficient first-order rate constants vs. T for CH_4 SR on composites promoted by $Pr_{0.3}Ce_{0.35}Zr_{0.35}O_2$ (1), $Pr_{0.15}La_{0.15}Ce_{0.35}Zr_{0.35}O_2$ (2), $Pr_{0.25}Ce_{0.5}Zr_{0.25}O_2$ (3), $Pr_{0.15}La_{0.15}Ce_{0.5}Zr_{0.2}O_2$ (4), $Pr_{0.15}Sm_{0.15}Ce_{0.35}Zr_{0.35}O_2$ (5) and $Pr_{0.15}Sm_{0.15}Ce_{0.5}Zr_{0.2}O_2$ (6). Feed 8% CH_4 + 8% H_2O in He, 10 ms contact time, O_2 pretreatment.

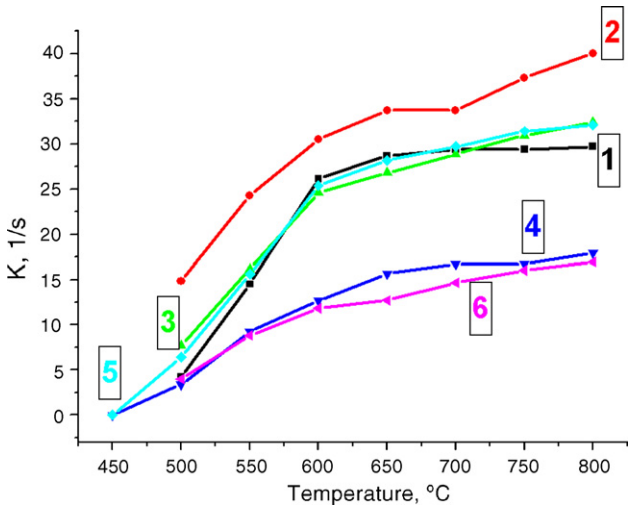

Fig. 8. Efficient first-order rate constants vs. *T* for CH_4 SR on composites promoted with fluorite-like oxides and 0.9 wt.% Ru. 8% CH_4 + 8% H_2O in He, 10 ms contact time, O_2 pretreatment. Type of oxide promoters: (1) $Pr_{0.3}Ce_{0.35}Zr_{0.35}O_2$; (2) $Pr_{0.15}La_{0.15}Ce_{0.35}Zr_{0.35}O_2$; (3) $Pr_{0.25}Ce_{0.5}Zr_{0.25}O_2$; (4) $Pr_{0.15}La_{0.15}Ce_{0.5}Zr_{0.2}O_2$; (5) $Pr_{0.15}Sm_{0.15}Ce_{0.35}Zr_{0.35}O_2$; (6) $Pr_{0.15}Sm_{0.15}Ce_{0.5}Zr_{0.2}O_2$.

an active metal in combination with fluorite-like oxides if a good decoration of its surface by these oxide promoters is achieved. A high catalytic activity of small NiO clusters stabilized on the surface of fluorite-like oxide promoters could be possible as well [17]. In these cases, activated CH_x fragments generated on Ni are rapidly transformed into CO and H_2 by interaction with hydroxyls or hydroxocarbonates supplied by the oxide promoters. In turn, these species are generated by water and CO_2 adsorption and activation on the surface sites of these complex oxides. Perhaps, redox properties of oxide promoters as well as their basicity play also an important role in this interaction of hydroxyls/hydroxocarbonates with CH_x fragments. Though pronounced rearrangement of composites microstructure in operation conditions [17] precludes any simple straightforward correlations between activity and oxygen mobility/reactivity in composites estimated by H_2 TPR, some general trends could be nevertheless outlined. First, samples possessing a high activity in the middle-temperature range (Fig. 7, curves 4 and 6) are among samples the most easily reduced by H_2 (Fig. 3, curves 4 and 5). A lower performance of composite promoted by La-containing complex oxide (Fig. 7, curve 4) as compared with that promoted by Sm-containing oxide (Fig. 7, curve 6) implies that too high basicity of the largest La cation hampers mobility and/or reactivity of hydroxocarbonate species. On the other hand, in the high-temperature range, the highest level of activity is observed for composites promoted by oxides containing only Pr, Ce and Zr cations (Fig. 7, curves 1 and 3). Perhaps, at high temperatures, where the rate of methane activation is very fast and the surface coverage by hydroxyls and carbonates declines due to desorption of water and CO_2, red-ox properties of promoting oxides play determining role in preventing coking of Ni surface.

In general, Ru-supporting promotes performance of composites in stoichiometric feed (Fig. 8). This certainly correlates with much faster reduction of Ru-promoted composites by H_2 (vide supra), suggesting increased surface/near-surface oxygen mobility. In addition, formation of Ru–Ni surface alloy might prevent coking of Ni surface [17]. However, in general, effects of Ru addition on activity in CH_4 SR could broadly vary due to pronounced variation of samples microstructure. Thus, for systems efficient in the middle-temperature range without Ru, effect of Ru supporting is either weak or absent. Since for these systems the most strong stabilization of RuO_x species by oxidic components is observed, including, probably, Ru incorporation into domain boundaries of NiO particles, fluorite-like oxides or nanopores of YSZ (vide supra), a moderate activity of these composites promoted by Ru can be assigned to a low surface concentration of metallic Ru particles efficient in methane activation. This conclusion agrees with the highest activity of composite co-promoted by Ru and $Pr_{0.15}La_{0.15}Ce_{0.35}Zr_{0.35}O_2$ oxide. Indeed, this sample is characterized by the intermediate reduction characteristics of RuO_x surface species (Fig. 6, curve 3), so in the reaction conditions its surface contains Ru clusters both highly active in CH_4 activation and stabilized by support to prevent their aggregation or coking.

The increase of Ru content from 0.9 to 1.3 wt.% decreases composite performance in stoichiometric feed in nearly all temperature range (Fig. 9). This is explained by the fact that stable performance of these composites is determined by the balance between accumulation of surface carbon-containing species–coke precursors generated on Ni and Ru centers, and their gasification due to interaction with oxygen-containing species generated on complex oxide components. Apparently, the increase of Ru loading increases the rate of carbon accumulation, while the rate of their gasification at least remains constant, hence, the overall decrease of performance is observed due to coking. The increase of steam content in the feed increases performance of composite promoted by 1.3 wt.% Ru, which is clearly explained by removal of coke from the surface in more oxidizing conditions. For sample promoted by 0.9 wt.% Ru, more complex effects are observed when increasing steam excess in the feed: activity declines at lower temperatures and increases at high temperatures (Fig. 9). Decline of activity in the low-temperature range in feeds with the excess of steam was also observed in the case of Ni–YSZ composites co-promoted by Pd and fluorite-like complex oxides and explained by stabilization of less reactive oxidic Pd forms due to interaction with oxide promoters [18,19]. Hence, for samples promoted by Ru, performance is strongly affected by the content of Ru and feed composition, both too oxidizing and too reducing conditions being not favorable for a high performance in some range of temperature.

3.2.2. Ethanol steam reforming

In this reaction, in general, in the middle-temperature range, activity of all composites, promoted by Ru or not, was rather high (Fig. 10). This is explained by a high activity of Ni in this reaction

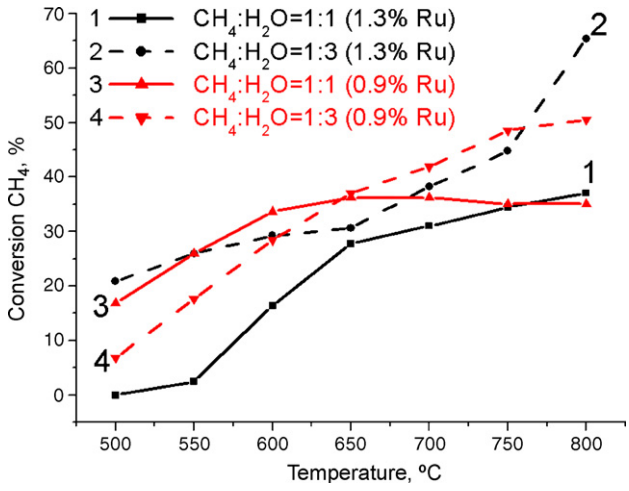

Fig. 9. Effect of steam/CH_4 ratio in the feed (CH_4 content 8%) on CH_4 conversion for composite 10% $Pr_{0.15}La_{0.15}Ce_{0.35}Zr_{0.35}O_2$/NiO + YSZ promoted with 1.3 wt.% Ru (1 and 2) or 0.9 wt.% Ru (3 and 4).

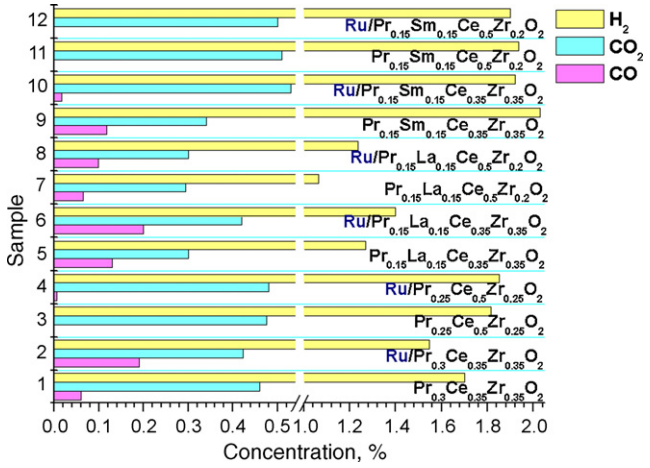

Fig. 10. Concentration of products in the steam reforming of ethanol on composites promoted with fluorite-like oxides and 0.9 wt.% Ru. 700 °C, contact time 0.036 s.

provided coking of its surface is hindered by oxidic promoters [5,4]. Moreover, specific activity of Ni supported on alumina is reported to be even higher than that of low-loaded Ru [4,5,10]. This agrees with the results of Srinivas et al. [26] demonstrating a high and stable activity in ESR of composites comprised of 40 wt.% NiO and 60 wt.% CeO_2 (CeO_2–ZrO_2) prepared via hydrothermal route. Hence, promoted composites efficient and stable in steam reforming of methane are also quite promising for the steam reforming of ethanol. As can be inferred from the hydrogen content in converted feed, at 700 °C, even at short contact time, up to 70% of ethanol is converted along the steam reforming route. Since breaking of C–C bond in the ethanol molecule is less demanding than in the case of C–H bond in methane molecule, this could be one of the reasons of rather weak structural sensitivity of this reaction as related to hydrogen yield.

Experiments with realistic feed composition (10% EtOH, vide supra experimental) confirmed a high performance and stability to coking (at least for 10–20 h of time-on stream) for one of the best composites (Fig. 11). In these experiments, ethanol conversion exceeds 92% achieving complete conversion at 800 °C. In agreement with earlier results for Ni-based composites [25,26], the main by-product is CH_4 (selectivity up to 25% at 600 °C), with only traces of methanol being revealed. Appearance of methanol as by-product certainly suggests that cracking of some ethanol-derived

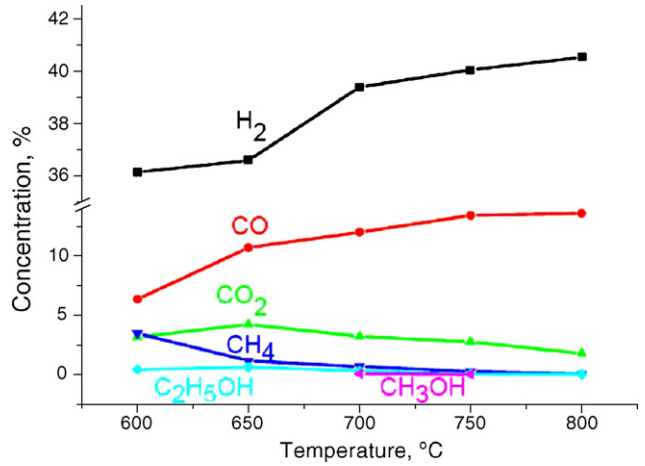

Fig. 11. Product distribution for steam reforming of ethanol on 0.9 wt.% Ru/$Pr_{0.15}Sm_{0.15}Ce_{0.35}Zr_{0.35}O_2$/NiO + YSZ sample. Feed composition EtOH:H_2O:N_2 = 1:4:5.

surface species (perhaps, acetates located on support sites adjacent to the metal ones [36]) takes place. However, such a cracking of acetates usually produces CH_4 and not CH_3OH [36]. Hence, for composite catalysts of the type considered in this work, the efficient interaction of CH_3 radicals produced by such a cracking with hydroxyls supplied by the complex oxide promoter or YSZ might be speculated as a possible route explaining appearance of methanol traces in products. Note that even at rather short contact times (70 ms), C_2H_4 was not revealed in the products, while it was inevitably present for catalysts comprised of precious metals supported on alumina [5,6,25,36]. Hence, for developed in this work composite systems containing YSZ and complex fluorite-oxide promoters, the primary route of ethanol transformation into syngas seems not to include ethanol dehydration. This agrees with very high CO_2/CO ratio in products at 700 °C in diluted feed clearly not conforming to the equilibrium composition of converted feed [26] or to results obtained with a high content of ethanol in the feed rather close to equilibrium at high temperatures (Fig. 11). Absence or very low concentration of CO in products for composites promoted by oxides with a high Ce content implies that red-ox properties of promoters are also responsible for routes of ethanol transformation into carbon oxides [35,36]. Since at high temperatures acetates are the only surface species detected by infra-red spectroscopy [36], at short contact times CO_2 can be considered as primary product of their decomposition.

For a sample discharged after ESR, temperature-programmed oxidation of deposited coke (Fig. 12, curve 1) revealed rather low amount of carbonaceous species (close to earlier estimated values for composite samples after operation in stoichiometric methane/steam feed [17]) rather easily removed at temperatures below 350 °C. According to the usual assignment [25], this peak corresponds to oxidation of superficial carbon in close contact with the metallic particles. Since this sample possesses the lowest performance in the ethanol steam reforming (Fig. 10), a lower carbon coverages for more active samples could be expected. Moreover, in fact, due to applied procedure of cooling samples in the reaction atmosphere before TPO tests clearly favoring additional coking at low temperatures (see Section 2), thus estimated amount of deposited carbon could be in fact several times bigger than the actual content of carbonaceous deposits in the steady-state conditions at operational temperatures.

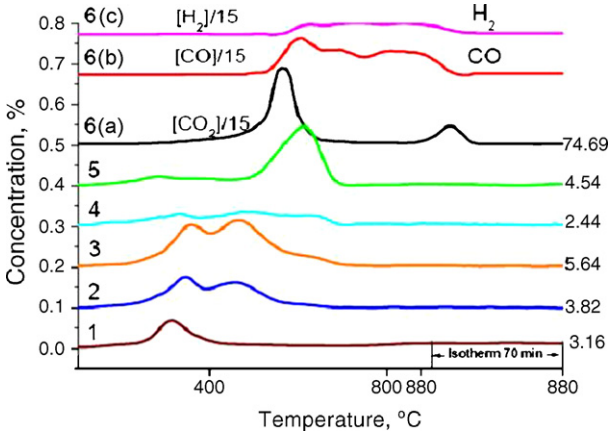

Fig. 12. Typical curves of CO_2 (1–6a), CO (6b) and H_2 (6c) evolution during temperature-programmed oxidation of carbonaceous deposits for some studied samples of composites promoted by $Pr_{0.15}La_{0.15}Ce_{0.5}Zr_{0.2}O_2$ (1), $Pr_{0.15}La_{0.15}Ce_{0.5}Zr_{0.2}O_2$ (2), $Pr_{0.15}Sm_{0.15}Ce_{0.35}Zr_{0.35}O_2$ (3), 0.9 wt.% Ru + $Pr_{0.15}La_{0.15}Ce_{0.35}Zr_{0.35}O_2$ (4), 1.3 wt.% Ru + $Pr_{0.15}La_{0.15}Ce_{0.35}Zr_{0.35}O_2$ (5) and $Pr_{0.15}La_{0.15}Ce_{0.35}Zr_{0.35}O_2$ (6) discharged after reaction of ethanol (1) or acetone (2–6) steam reforming. Amount of removed carbon (mmol/g) is indicated at the right end of each curve.

More detailed analysis allowed to assess the relative importance of different factors responsible for the composite performance in ethanol steam reforming in diluted feed.

As far as the effect of fluorite-like additives is concerned, the highest activity was demonstrated by composites promoted with Sm-containing oxides, while La-containing additives demonstrated the lowest yields of hydrogen. According to H_2 TPR data, a higher reducibility, and, hence, lattice oxygen mobility is revealed for composites promoted by Sm-containing oxides, while the lowest for those containing La cations (vide supra). This suggests that the most important factor responsible for a high activity of promoted composites in steam reforming of ethanol is the oxygen mobility of oxide additives preventing catalysts deactivation by coke deposition [10].

Supporting Ru on $Pr_{0.15}Sm_{0.15}Ce_{0.5}Zr_{0.2}O_2$ composite slightly decreases hydrogen yield which can be assigned to somewhat higher yield of CH_4 due to reaction of CO (CO_2) methanation [6]. For composite promoted by $Pr_{0.15}Sm_{0.15}Ce_{0.35}Zr_{0.35}O_2$, co-promotion with Ru increases CO_2 yield but decreased CO and H_2 yield, which can be explained by a higher conversion of ethanol on Ru-containing sample along with preferential CO methanation. Hence, at short contact times and in diluted feeds, the water gas shift reaction is apparently not equilibrated.

When Ru was supported on less active composites promoted by La-containing oxides, another effects were observed: both hydrogen and CO_x yields were increased. While the increase of CO yield can be assigned to acceleration of reverse water gas shift reaction catalyzed by Ru particles weakly interacting with promoting fluorite-like oxides in these composites (vide supra), the increase of hydrogen and CO_2 content in the feed suggests that the overall transformation of ethanol along the steam reforming route is accelerated as well, perhaps, due to decreasing the surface coking and/or accelerating other stages of intermediates (acetate, methane, etc.) transformation into hydrogen and carbon oxides as was demonstrated by similar increase of the middle-temperature performance in steam reforming of methane (vide supra).

Hence, for ethanol steam reforming reaction, the effect of supported promoters (complex fluorite-like oxides and Ru) also depends upon their combinations despite reasonably high activity of promoted Ni in these composites by itself. For this reaction, the structural sensitivity is also revealed despite much easier activation of ethanol than methane via ethoxide intermediates [36]. Apart from the effects of oxygen mobility and redox activity of promoting complex oxides affecting both overall performance and CO selectivity, more specific action of Ru able to catalyze different stages of the overall catalytic reaction could be important as well. This means that any combinatorial strategy of synthesis of active components for ethanol steam reforming reactions should take into account not only their chemical composition but structural arrangement as well.

3.2.3. Acetone steam reforming

In the reaction of acetone steam reforming concentrations of H_2 and CO_x were chosen as parameters characterizing catalytic activity along the steam reforming route. In majority of cases, some amount of methane was detected at 500 °C, while it disappeared at higher temperatures. This indicates that cracking of acetone occurs yielding methane as by-product. When after attainment of a steady-state at 500 °C the temperature was increased by a step of 100 °C from 500 to 700 °C, H_2 concentration was increased and CO_2 concentration declined, achieving a new stationary level within ~10 min. On the other hand, at each step, CO concentration was first rapidly increased following the same time scale ~10 min, then slowly (~60 min) declined to a new stationary level which can be somewhat higher or lower as compared with the level obtained at a previous temperature of experiment (not shown for brevity). This behavior implies that some progressive coking of the surface happens with the increase of the temperature leading to decline of the rate of transformation of surface compounds into CO. At the same time, generation of hydrogen and CO_2, perhaps occurring on sites of a different nature (site of support in close contact with metal particles) depends rather weakly upon the surface coking in the time scale of these experiments. According to results of Vargas et al. [35], deactivation of Ce–Zr–Co fluorite-type oxide catalysts in steam reforming of ethanol due to coking was accompanied by going of acetone concentration in products through the maximum and continuous increase of CH_3CHO concentration, while concentrations of H_2 and CO_2 were practically constant and that of CO slowly declined. Similarity with the dynamics observed in our case suggests that at higher temperatures a part of acetone is transformed into hydrogen and some short-chain oxygenates such as CH_3CHO, formic acid, etc. which are retained in the cold trap after reactor. Since there are practically no data published on the mechanism of acetone steam reforming, this question certainly deserves further studies. However, we should stress that for all samples, the level of activity achieved at a given temperature was constant for at least 2–3 h, hence, it corresponds to a steady-state in applied experimental conditions. This implies that a steady-state surface coverage by coke precursors is achieved due to parallel occurrence of reactions leading to coke generation and its gasification by steam.

Steady-state concentrations of products for some samples of studied series are shown in Fig. 13. As follows from these data, the maximum yield of H_2 is obtained for composite co-promoted with $Pr_{0.15}Sm_{0.15}Ce_{0.35}Zr_{0.35}O_2$ and 0.9% Ru, while the lowest yield is obtained for samples promoted by $Pr_{0.15}La_{0.15}Ce_{0.35}Zr_{0.35}O_2$ oxides with the lowest reducibility (cf. Fig. 3). This fact is in a good agreement with the results obtained for steam reforming of ethanol as well as methane (vide supra) thus evidencing again importance of the lattice oxygen mobility in promoted composites required to prevent coking.

Indeed, as follows from analysis of our dynamics data, TPO results (Fig. 12) as well as published results [23], for the reaction of acetone steam reforming coking appears to be more important problem than for the reaction of ethanol steam reforming. For samples discharged after acetone steam reforming (Fig. 12), the amount of deposited carbon is usually bigger than for sample

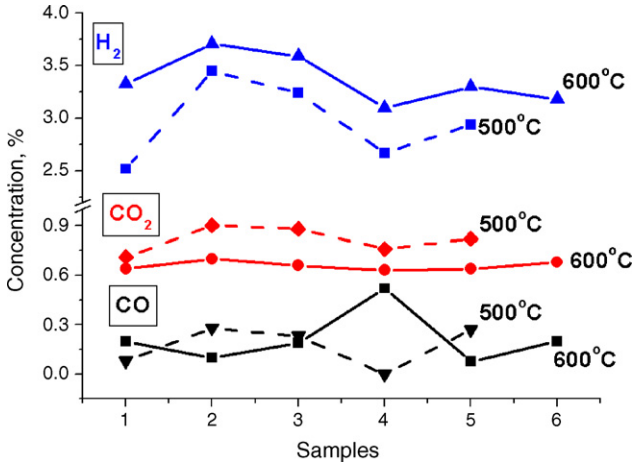

Fig. 13. Concentration of products in the steam reforming of acetone at 500 °C and 600 °C for different composites: (1) $Pr_{0.15}Sm_{0.15}Ce_{0.35}Zr_{0.35}O_2$; (2) Ru/$Pr_{0.15}Sm_{0.15}Ce_{0.35}Zr_{0.35}O_2$; (3) $Pr_{0.15}La_{0.15}Ce_{0.5}Zr_{0.2}O_2$; (4) $Pr_{0.15}La_{0.15}Ce_{0.35}Zr_{0.35}O_2$; (5) 0.9 wt.% Ru/$Pr_{0.15}La_{0.15}Ce_{0.35}Zr_{0.35}O_2$; (6) 1.3 wt.% Ru/$Pr_{0.15}La_{0.15}Ce_{0.35}Zr_{0.35}O_2$.

discharged after ethanol steam reforming, and new peaks of CO_2 evolution situated at higher temperatures usually assigned to oxidation of filamentous carbon [25] appear. The highest amount of deposited carbonaceous species was revealed for composite promoted by $Pr_{0.15}La_{0.15}Ce_{0.35}Zr_{0.35}O_2$ oxide (Fig. 12, curve 6a) with the lowest oxygen mobility (Fig. 3) and the lowest activity at 600 °C (Fig. 13). Their oxidation proceeds with evolution of not only CO_2 as found for all other samples, but CO and H_2 as well (Fig. 12, curves 6b and 6c). This suggests that these carbonaceous species also contain appreciable amount of hydrogen atoms.

For composite co-promoted by 0.9 wt.% Ru and $Pr_{0.15}La_{0.15}Ce_{0.35}Zr_{0.35}O_2$ oxide, the amount of deposited carbon is drastically decreased (Fig. 12, curve 4), which is reflected in the increase of hydrogen yield (Fig. 13). As was considered for the case of methane steam reforming (vide supra), both increase of the oxygen mobility due to Ru incorporation into the surface layers of complex fluorite-like oxide and formation of surface Ru–Ni alloys more resistant to coking could be responsible for these effects. Similarly for the case of methane steam reforming in the stoichiometric feed, the increase of Ru content from 0.9 to 1.3% decreases hydrogen yield (Fig. 13), which correlates with the increase of the amount of deposited carbon (Fig. 12, curve 5). In this case, not only the amount of deposited carbon but its reactivity might be important for composites performance. Indeed, for sample promoted by 1.3 wt.% Ru less reactive (and, perhaps, more dense) forms of carbonaceous deposits oxidized at temperatures exceeding 600 °C dominate (Fig. 12), so their gasification by steam may be difficult as well. Samples promoted only by complex oxides $Pr_{0.15}La_{0.15}Ce_{0.5}Zr_{0.2}O_2$ or $Pr_{0.15}Sm_{0.15}Ce_{0.35}Zr_{0.35}O_2$ and demonstrating a higher reducibility/lattice oxygen mobility as compared with composite promoted by $Pr_{0.15}La_{0.15}Ce_{0.35}Zr_{0.35}O_2$ (Fig. 3) are characterized by much smaller amount of deposited carbon oxidized at lower temperatures (Fig. 12, curves 2 and 3). Despite a bigger amount of deposited coke than for composite co-promoted by 0.9 wt.% Ru and $Pr_{0.15}La_{0.15}Ce_{0.35}Zr_{0.35}O_2$ oxide (Fig. 12), samples with a higher lattice oxygen mobility demonstrate a higher hydrogen yield (Fig. 13, samples 1 and 3) as compared with the former composite (Fig. 13, sample 4). This feature can be explained by a higher reactivity of carbonaceous species deposited on the surface of composite without Ru, which facilitates their gasification by steam. For composites without Ru, a lower amount of deposited coke (Fig. 12, curves 2 and 3) corresponds to a higher performance (hydrogen yield) for the sample promoted by complex oxide with a higher content of reducible Ce and Pr cations (Fig. 13, samples 1 and 3). However, even for composites promoted by oxides with a high lattice oxygen mobility co-promotion by 0.9 wt.% Ru allows to increase the hydrogen yield (Fig. 13, samples 1 and 2), which can be explained by factors considered above.

In general, the scale of variation of hydrogen yield within studied series of samples in acetone steam reforming (Fig. 13) is comparable with that for ethanol steam reforming (Fig. 10). The main difference between these two reactions is that for the former supporting 0.9% Ru increases hydrogen yield, similar to that for the case of methane steam reforming, while for the latter Ru supporting on composites promoted by Sm-containing complex oxides decreases it. The difference is apparently explained by more difficult activation of acetone molecule, including rupture of C–H bond which is facilitated by Ru as in the case of methane steam reforming.

At 500 °C, concentrations of all products vary in parallel in studied series of samples, reflecting their intrinsic catalytic properties after standard pretreatment in hydrogen. At higher temperatures, this parallelism disappears due to progressive surface coking considered above. Nevertheless, in any case, for used feed and studied temperature range, hydrogen and carbon dioxide are main products into which at least 50% of acetone in the feed is converted at short contact times at temperatures as low as 500 °C. Taking into account that such model biofuel as acetic acid is easily converted into acetone on zirconia, while subsequent transformation of acetone was found to be the main cause of ZrO_2-supported Pt deactivation due to coking, promoted nano-composites could be really promising for steam reforming of bio-oil containing organic acids. Certainly more detailed studies of the most promising compositions in realistic feeds are required to assess their performance and stability for the practical application.

4. Conclusions

Robotic workstation was successfully applied for synthesis of a series of YSZ + NiO composites co-promoted by complex doped fluorite-like ceria–zirconia oxides and Ru. This multistage preparation procedure based upon consecutive impregnation of YSZ powder with the excess of solutions of other components followed by evaporation and calcination resulted in strong interaction between components of composites reflected in such phenomena as decoration, redistribution of elements between different phases and variation of their structural features, reactivity and oxygen mobility as revealed by TEM with EDX, XRD and H_2 TPR. Promoted composites demonstrate a stable and broadly varying activity in the reactions of methane, ethanol and acetone steam reforming in stoichiometric feeds explained with a due regard for decreasing Ni coking due to positive effect of the oxygen mobility in complex oxide promoters, redox and acid–base properties of doping cations in complex oxide promoters and their ability to stabilize different types of Ru clusters/species taking part in activation of methane and oxygenates. Within studied series of composites, the scale of their catalytic performance variation is determined by the relative ease of fuel molecule activation, being the broadest for steam reforming of methane. The most promising systems for oxygenates and methane steam reforming possessing a high performance and stability to coking contain as promoters ceria–zirconia solid solutions with Ce/Zr ratio > 1 co-doped with Pr and Sm cations.

Acknowledgements

The authors acknowledge the financial support of INTAS YSF 06-1000014-5773, INTAS 05-1000005-7663, NATO SFP 980878, FP6 SOFC 600 Projects and Integration Project 95 SB RAS-NAN Ukraine.

References

[1] A. Demibras, Prog. Energy Comb. Sci. 33 (2007) 1.
[2] M. Asadullah, S. Ito, K. Kunimori, M. Yamada, K. Tomishige, J. Catal. 208 (2002) 255.
[3] W. Jamsak, S. Assabumrungrat, P.L. Douglas, N. Laosiripojana, R. Suwanwarangkul, S. Charojrochkul, E. Croiset, Chem. Eng. J. 133 (2007) 187.
[4] A.N. Fatsikostas, D.I. Kondarides, X.E. Verykios, Catal. Today 75 (2002) 145.
[5] A. Haryanto, S. Fernando, N. Murali, S. Adhikari, Energy Fuels 19 (2005) 2098.
[6] P. Breen, R. Burch, H.M. Coleman, Appl. Catal. B: Environ. 39 (2002) 65.
[7] M.C.J. Bradford, M.A. Vannice, J. Catal. 173 (1998) 157.
[8] M.M.V.M. Souza, M. Schmal, Appl. Catal. A: Gen. 255 (2003) 83.
[9] V.A. Sadykov, T.G. Kuznetsova, Yu.V. Frolova, G.M. Alikina, A.I. Lukashevich, V.A. Rogov, V.S. Muzykantov, L.G. Pinaeva, E.M. Sadovskaya, Yu.A. Ivanova, E.A. Paukshtis, N.V. Mezentseva, L.Ch. Batuev, V.N. Parmon, S. Neophytides, E. Kemnitz, K. Scheurell, C. Mirodatos, A.C. van Veen, Catal. Today 117 (2006) 475.
[10] M.C. Sanchez-Sanchez, R.M. Navarro, J.L.G. Fierro, Catal. Today 129 (2007) 336.
[11] P.Y. Sheng, W.W. Chiu, A. Yee, S.J. Morrison, H. Idriss, Catal. Today 129 (2007) 313.
[12] A.M. Silva, A.P.M.G. Barandas, L.O.O. Costa, L.E.P. Borges, L.V. Mattos, F.B. Noronha, Catal. Today 129 (2007) 297.
[13] J.-L. Bi, Y.-Y. Hong, C.-C. Lee, C.-T. Yeh, C.-B. Wang, Catal. Today 129 (2007) 322.
[14] C. Diagne, H. Idriss, A. Kiennemann, Catal. Commun. 3 (12) (2002) 565.
[15] J.A. Montoya, E. Romero-Pascual, C. Gimon, P.D. Angel, Catal. Today 63 (2000) 71.
[16] V.A. Sadykov, T.G. Kuznetsova, Yu.V. Frolova, et al. Catal. Today 117 (2006) 475.
[17] V.A. Sadykov, N.V. Mezentseva, R.V. Bunina, G.M. Alikina, A.I. Lukashevich, T.S. Kharlamova, V.A. Rogov, V.I. Zaikovskii, A.V. Ishchenko, T.A. Krieger, O.F. Bobrenok, A. Smirnova, J. Irvine, O.D. Vasylyev, Catal. Today 131 (2008) 226.

[18] V.A. Sadykov, N.V. Mezentseva, R.V. Bunina, Mater. Res. Soc. Symp. Proc. 972 (2007) AA03–AA06.
[19] V. Sadykov, N. Mezentseva, G. Alikina, A. Lukashevich, V. Muzykantov, R. Bunina, A. Boronin, E. Pazhetnov, E. Paukshtis, V. Kriventsov, A. Smirnova, O. Vasylyev, J. Irvine, O. Bobrenok, V. Voronin, I. Berger, Mater. Res. Soc. Symp. Proc. 1023 (2007) JJ02–JJ07.
[20] V.A. Sadykov, N.V. Mezentseva, G.M. Alikina, A.I. Lukashevich, Yu.V. Borchert, T.G. Kuznetsova, V.P. Ivanov, S.N. Trukhan, E.A. Paukshtis, V.S. Muzykantov, V.L. Kuznetsov, V.A. Rogov, J. Ross, E. Kemnitz, K. Sheurell, Solid State Phenom. 128 (2007) 239.
[21] V.A. Sadykov, N. Mezentseva, G. Alikina, A. Lukashevich, V. Muzykantov, T. Kuznetsova, L. Batuev, M. Fedotov, E. Moroz, D. Zyuzin, V. Kolko, V. Kriventsov, V. Ivanov, A. Boronin, E. Pazhetnov, V. Zaikovskii, A. Ishchenko, V. Rogov, J. Ross, E. Kemnitz, Mater. Res. Soc. Symp. Proc. 988 (2007) QQ04–QQ06.
[22] G. Grasso, B. Harji, E. Xue, S. Belochapkine, J.R.H. Ross, Catal. Today 81 (2003) 369.
[23] K. Takanabe, K. Aika, K. Seshan, L. Lefferts, J. Catal. 227 (2004) 101.
[24] D.A. Zyuzin, S.V. Cherepanova, E.M. Moroz, E.B. Burgina, V.A. Sadykov, V.G. Kostrovskii, V.A. Matyshak, J. Solid State Chem. 179 (2006) 2965.
[25] F. Romero-Sarria, J.C. Vargas, A.-C. Roger, A. Kiennemann, Catal. Today 133–135 (2008) 149.
[26] D. Srinivas, C.V.V. Satyanarayana, H.S. Potdar, P. Ratnasamy, Appl. Catal. A: Gen. 246 (2003) 323–334.
[27] J.A. Montoya, E. Romero-Pascual, C. Gimon, P. Del Angel, A. Monzon, Catal. Today 63 (2000) 71.
[28] Y. Matsumura, T. Nakamori, Appl. Catal. A: Gen. 258 (2004) 107.
[29] F. Pompeo, N.N. Nichio, M.M.V.M. Souza, D.V. Cesar, O.A. Ferretti, M. Schmal, Appl. Catal. A: Gen. 316 (2007) 175.
[30] S.N. Pavlova, N.N. Sazonova, V.A. Sadykov, O.I. Snegurenko, V.A. Rogov, E.M. Moroz, A.V. Simakov, V.N. Parmon, Kinet. Catal. 45 (2004) 589.
[31] S. Bernal, J.J. Calvino, J.M. Gatica, C.L. Cartes, J.M. Pintado, Catalysis by ceria and related materials, in: A. Trovarelli (Ed.), Catalytic Science Series, vol. 2, Imperial College Press, London, UK, 2002, pp. 85–168.
[32] E.M. Sadovskaya, Y.A. Ivanova, L.G. Pinaeva, G. Grasso, T.G. Kuznetsova, A. van Veen, V.A. Sadykov, C. Mirodatos, J. Phys. Chem. A 111 (2007) 4498.
[33] A. Yan, B. Liu, B. Tu, Y. Dong, M. Cheng, Sh. Song, P. Tsiakaras, J. Fuel Cell Sci. Technol. 4 (2007) 79.
[34] S. Hosokawa, H. Kanai, K. Utani, Y. Taniguchi, Y. Saito, S. Imamura, Appl. Catal. B: Environ. 45 (2003) 181.
[35] J.C. Vargas, S. Libs, A.-C. Roger, A. Kiennemann, Catal. Today 107–108 (2005) 417.
[36] A. Erdőhelyi, J. Raskó, T. Kecskés, M. Tóth, M. Dömök, K. Baán, Catal. Today 116 (2006) 367.